Comparison of contraction and calcium handling between right and left ventricular myocytes from adult mouse heart: a role for repolarization waveform

Richard P. Kondo[1,2], Dorothy A. Dederko[2], Christine Teutsch[1,2], Jacqueline Chrast[2], Daniele Catalucci[1,2], Kenneth R. Chien[2] and Wayne R. Giles[3,2]

Departments of [1] Medicine and [2] Bioengineering and [3] Institute of Molecular Medicine, University of California, San Diego, La Jolla, CA, USA

In the mammalian heart, the right ventricle (RV) has a distinct structural and electrophysiological profile compared to the left ventricle (LV). However, the possibility that myocytes from the RV and LV have different contractile properties has not been established. In this study, sarcomere shortening, $[Ca^{2+}]_i$ transients and Ca^{2+} and K^+ currents in unloaded myocytes isolated from the RV, LV epicardium (LVepi) and LV endocardium (LVendo) of adult mice were evaluated. Maximum sarcomere shortening elicited by field stimulation was graded in the order: LVendo > LVepi > RV. Systolic $[Ca^{2+}]_i$ was higher in LVendo myocytes than in RV myocytes. Voltage-clamp experiments in which action potential (AP) waveforms from RV and LVendo were used as the command signal, demonstrated that total Ca^{2+} influx and myocyte shortening were larger in response to the LVendo AP, independent of myocyte subtypes. Evaluation of possible regional differences in myocyte Ca^{2+} handling was based on: (i) the current–voltage relation of the Ca^{2+} current; (ii) sarcoplasmic reticulum Ca^{2+} uptake; and (iii) mRNA expression of important components of the Ca^{2+} handling system. None of these were significantly different between RV and LVendo. In contrast, the Ca^{2+}-independent K^+ current, which modulates AP repolarization, was significantly different between RV, LVepi and LVendo. These results suggest that these differences in K^+ currents can alter AP duration and modulate the $[Ca^{2+}]_i$ transient and corresponding contraction. In summary, these findings provide an initial description of regional differences in excitation–contraction coupling in the adult mouse heart. Evidence that the AP waveform is an important causative factor for these differences is presented.

(Resubmitted 4 November 2005; accepted after revision 9 December 2005; first published online 15 December 2005)
Corresponding author W. R Giles: Department of Bioengineering, Whitaker Institute of Biomedical Engineering, PFBG 384, University of California, San Diego, 9500 Gilman Drive, La Jolla, CA 92093-0412, USA.
Email: wgiles@bioeng.ucsd.edu

In hearts from adult mammals, right (RV) and left (LV) ventricles have distinctive structural and contractile characteristics as well as heterogeneous electrophysiological properties (Katz, 2001). The RV pumps blood into the relatively low-pressure pulmonary vasculature. Accordingly RV chamber pressures are much lower and the workload of the right ventricle (RV) differs significantly from that of the left ventricle (LV). In addition, the mechanical afterload in the right ventricle is significantly smaller. Consistent with these physiological differences, the free wall of the RV is much thinner than that of the LV. Systematic electrophysiological studies have also shown that the mammalian ventricle exhibits a well-defined heterogeneity of AP waveforms. In adult mice and rats, the AP duration (APD) at a fixed heart rate is shorter in the RV than in the LV (Watanabe *et al.* 1983; Clark *et al.* 1993; Knollmann *et al.* 2001) while in larger mammals, the notch during phase 1 of the AP is deeper in the RV than in the LV (Di Diego *et al.* 1996). A major reason for these differences is the higher density of transient outward potassium current ($I_{to,f}$) in the RV (Di Diego *et al.* 1996; Rosati *et al.* 2003; Brunet *et al.* 2004). While these RV–LV electrophysiological differences have been demonstrated in a number of species, their effects on contractile activity have not been explored systematically (Grattan *et al.* 2005).

In cardiac muscle, trans-sarcolemmal Ca^{2+} influx is an essential prerequisite for contraction (Nabauer *et al.* 1989), although in mammalian ventricle, the majority of Ca^{2+} used for activating the contractile apparatus is released from the sarcoplasmic reticulum (SR) (Wier, 1990; Barry & Bridge, 1993; Bers, 2001). In the steady state,

 DOI: 10.1113/jphysiol.2005.101428

contractile strength at a fixed heart rate in response to synchronous activation reflects a balance between the Ca^{2+} influx plus SR Ca^{2+} release, and Ca^{2+} efflux and SR-mediated uptake of Ca^{2+} during diastole. Contractile strength is also strongly modulated by length-dependent Ca^{2+} sensitivity of the contractile proteins (Solaro & Rarick, 1998). Repolarizing K^+ currents can indirectly modulate contraction by altering AP profile and duration and hence changing intracellular $[Ca^{2+}]$ dynamics (Wood *et al.* 1969; Fiset *et al.* 1997; Volk *et al.* 1999; Bassani *et al.* 2004). In particular, it has been proposed that $I_{to,f}$ affects contraction by changing the AP profile and therefore modulates L-type Ca^{2+} current ($I_{Ca,L}$) during the early phase of repolarization (Bouchard *et al.* 1995; Volk *et al.* 1999; Sah *et al.* 2003). In rodents, the density of $I_{to,f}$ is relatively high (Fiset *et al.* 1997; Xu *et al.* 1999). Partly for this reason, the rodent AP repolarizes rapidly and does not have a distinctive plateau phase. In previous experiments using ventricular myocytes from rodents, slowing of the repolarization rate of the AP resulted in an enhanced $I_{Ca,L}$ and larger contraction (Bouchard *et al.* 1995). In rodents and larger mammals, the APD of the LV is longer than that of the RV (Watanabe *et al.* 1983; Clark *et al.* 1993; Di Diego *et al.* 1996; Knollmann *et al.* 2001). This raises the possibility that AP waveform modulates the contractile strength of LV myocytes such that LV contraction is greater than that of RV at a fixed heart rate.

To determine whether this is the case, we have measured sarcomere shortening and $[Ca^{2+}]_i$ transients in myocytes isolated from RV, LV epicardium and LV endocardium of adult mouse hearts. The consistent finding was that maximal sarcomere shortening is significantly greater in unloaded LV endocardial myocytes than in RV myocytes and LV epicardial myocytes. $[Ca^{2+}]_i$ transients are also larger in LV endocardial myocytes compared to RV myocytes. These significant regional differences of excitation–contraction coupling in the adult mouse heart were the focus of this study.

Methods

Isolation of ventricular cells from right and left ventricles

The adult mouse ventricular myocyte isolation protocol was adopted from the method published by Brouillette *et al.* (2003). This protocol was approved by the Animal Subjects Committee at the University of California, San Diego. Male C57B6 mice (8–10 weeks) were killed using a sodium pentobarbital overdose by intraperitoneal injection (200 mg kg^{-1}). The hearts were excised and the aortas cannulated for retrograde perfusion with a sequence of four solutions, all of which were warmed to 37°C: (1) Tyrode solution containing (mM): NaCl 130, KCl 5.4, $CaCl_2$ 1, $MgCl_2$ 1, Na_2HPO_4 0.3, Hepes 10 and glucose 5.5; pH adjusted to 7.4 with NaOH) for 4–5 min; (2) Ca^{2+}-free Tyrode solution containing (mM): NaCl 130, KCl 5.4, $MgCl_2$ 1, Na_2HPO_4 0.3, Hepes 10 and glucose 5.5; pH 7.3 for 10 min; (3) Ca^{2+}-free Tyrode supplemented with 0.4 mg ml^{-1} collagenase (Worthington Type II), 30 μM $CaCl_2$, 0.1% bovine serum albumin (BSA; Sigma, Fraction V) and 20 mM taurine for 18 min; and (4) Ca^{2+}-free Tyrode solution supplement with 30 μM $CaCl_2$. Following this procedure, each heart was dissected as follows: (1) approximately 0.25 mm × 0.5 mm strips were prepared from the base region of the RV, LV subepicardium and LV subendocardium; (2) these tissue strips were digested with the same collagenase-containing solution for 5–8 min in separate flasks in a shaking water bath at 37°C. The tissue was collected in separate tubes containing Ca^{2+}-free Tyrode solution supplemented with 100 μM Ca^{2+}. Individual myocytes were released from the tissue by mechanical agitation, and then the populations of cells were washed using two complete cycles of low-speed centrifuge spin (IEC clinical no. 3 setting). This was followed by aspiration and addition of Ca^{2+}-free Tyrode solution supplemented with 0.2% BSA and increasing levels of $CaCl_2$: 200 μm and 600 μm. After this final spin, the isolated myocytes were stored in Tyrode solution containing (mM): NaCl 140, KCl 5.4, $MgCl_2$ 1, $CaCl_2$ 1, Hepes 10 and glucose 10; pH 7.4 at room temperature. Typical preparations contained 50–80% rod-shaped, quiescent, Ca^{2+}-tolerant myocytes which had well-defined, regular cross-striations and sarcomere patterns.

Shortening and $[Ca^{2+}]_i$ transients

Sarcomere length and $[Ca^{2+}]_i$ transients were recorded from single myocytes using an epi-fluorescence inverted microscope (Nikon TS100) with an attached CCD camera (Ionoptix MyoCam, Ionoptix, Milton, MA, USA). $[Ca^{2+}]_i$ was measured using a dual excitation spectrophotometer which detects the fluorescence excited by UV light at 340 and 380 nM. In these experiments, an aliquot of myocytes was placed into a small superfusion chamber which received Tyrode solution containing either 1.0 or 1.8 mM $CaCl_2$ at 19–21°C. All measurements were made on rod-shaped myocytes which had regular well defined striations. Myocytes were field stimulated using platinum electrodes. Steady-state trains of stimuli (2 ms) were applied at frequencies of 0.5, 1 and 2 Hz. Average sarcomere length within the user-determined window, was measured using the Ionoptix Ltd software that determines the average periodicity of the Z-line density based on the fast Fourier transform algorithm. Unloaded sarcomere shortening was calculated as the difference between peak systolic length and maximum diastolic length. Kinetic parameters for the shortening transient were determined using a curve-fitting algorithm (Ionoptix). $[Ca^{2+}]_i$ transients were measured using the ratiometric dye, fura-4F (Molecular Probe Ltd.). Fura-4F was chosen because it

has a lower affinity for Ca^{2+} than Fura-2. This reduced the possibility of significantly altering myoplasmic $[Ca^{2+}]$ by intrinsic dye-dependent buffering. The acetoxymethyl ester form of Fura-4F (2 μM) was dissolved in DMSO and added to an aliquot of myocytes for 20 min and then washed out with normal Tyrode solution. A 30-min time period was then allowed for de-esterification of the dye in the myoplasm. In some of the experiments, fluorescence and sarcomere shortening were measured simultaneously. Fluorescence ratios were calibrated using a modification of a published protocol (Williams & Fay, 1990) which requires determination of R_{min} and R_{max}, the fluorescence ratios of Fura-4F in a Ca^{2+}-free and Ca^{2+}-saturating intracellular environment, respectively. $[Ca^{2+}]_i$ is computed as $K_dB(R - R_{min})/(R_{max} - R)$ (Grynkiewicz *et al.* 1985) where B is the ratio of fluorescence of Ca^{2+}-free Fura-4F to Ca^{2+}-saturated Fura-4F excited by 380 nm. R_{min} was assessed in myocytes following complete metabolic inhibition (5- to 10-min exposure to 10 μM H+ Ionophore FCCP). The fluorescence ratio was determined in five myocytes after the $[Ca^{2+}]_i$ was clamped to very low levels by (i) removal of $[Ca^{2+}]_o$; and (ii) the addition of 10 mM EGTA and 2–5 μM ionomycin, a Ca^{2+} ionophore. Subsequently, $[Ca^{2+}]_o$ was restored to normal levels by the re-addition of 1 mM $[Ca^{2+}]_o$ and the removal of the EGTA. Finally, R_{max} was determined in five myocytes following the addition 2–5 μM ionomycin to insure rapid Ca influx in order to raise the $[Ca^{2+}]_i$ to millimolar levels. The K_d of Fura-4F for Ca^{2+} is 1.1 μM (Wokosin *et al.* 2004).

Voltage-clamp measurements

The total outward K^+ current and $I_{Ca,L}$ were recorded using the conventional whole-cell, voltage-clamp technique with an Axopatch 200B patch-clamp amplifier (Axon Instruments). Glass microelectrodes which were made from 1.5-mm capillary glass (WPI instruments, PG52151), were pulled to achieve a final pipette resistance of 1.5–2.5 MΩ when filled with one of the two patch pipette solutions. For K^+ current measurements, the pipette solution consisted of (mM): potassium aspartate 110, KCl 20, NaCl 8, $MgCl_2$ 1, $CaCl_2$ 1, EGTA 10, K_2ATP 4 and Hepes 10; pH 7.2, and the extracellular solution was Tyrode solution containing (mM): NaCl 140, KCl 5.4, $MgCl_2$ 1, $CaCl_2$ 1 and Hepes 10; pH 7.4. For recording $I_{Ca,L}$, the pipette solution contained (mM): CsCl 140, $MgCl_2$ 1, $CaCl_2$ 1, EGTA 5, Mg-ATP 4 , Hepes 5, TEA-Cl 10 and cAMP 0.1; pH 7.2. The isotonic replacement of K^+ by Cs^+ and the addition of TEA to the pipette solution for the measurements of $I_{Ca,L}$ was done to eliminate K^+ currents. In these experiments, the extracellular solution was a modified Tyrode solution containing (mM): NaCl 110, CsCl 5.4, $MgCl_2$ 1, $CaCl_2$ 1.8, TEA-Cl 30 and Hepes 10; pH 7.4, and 2.5 mM 4-aminopyridine (4-AP) was added to this solution to block total outward K^+ current. All whole-cell voltage-clamp recordings were performed at room temperature (19–21°C). Data were retained only if the initial series resistance following rupture was 15 MΩ or less. Series resistance was compensated (80–85%) and the capacitance of the myocyte was measured and subtracted. Membrane potentials were corrected for liquid junction potential by −10 mV (K^+ current experiments) or −5 mV (Ca^{2+} current studies). Total outward K^+ current was recorded during 500-ms depolarizing voltage steps from −50 to +30 mV from a holding potential (HP) of −80 mV (Fiset *et al.* 1997; Brouillette *et al.* 2004). The interval between voltage steps was set at 10 s in order to allow complete recovery of total outward K^+ current. $I_{Ca,L}$ was recorded in response to 500-ms depolarizing voltage steps from −50 to +45 mV from an HP of −40 mV. This HP strongly inactivated the large transient inward Na^+ current (I_{Na}). In these experiments, a 400-ms hyperpolarization to −80 mV was used to accelerate the recovery of $I_{Ca,L}$ and enhance Ca^{2+} extrusion (Bouchard *et al.* 1995). This voltage-clamp protocol was repeated at 2-s intervals. Peak I_{Ca} was determined as the difference between the peak inward current and the steady-state outward current at the end of the voltage-clamp pulse. Cell capacitance was determined by integrating capacitance transients recorded during a brief 5-mV step from an HP of −70 mV. The cell capacitance was calculated as the ratio of the integral of the capacitance transient divided by the voltage step (RV myocytes. The values were: 138 ± 9 pF (30); LV endo myocytes 158 ± 10 pF (33), P value: 0.14).

Ca^{2+} currents and myocyte shortening were recorded simultaneously during voltage-clamp experiments in which selected AP-like waveforms were used as the command signal. Figure 1 shows the AP waveforms that are representative of measured RV and LV endocardial AP (Knollmann *et al.* 2001). A sequence of 20–25 RV or LVendo AP clamps was applied at 2 Hz and the data

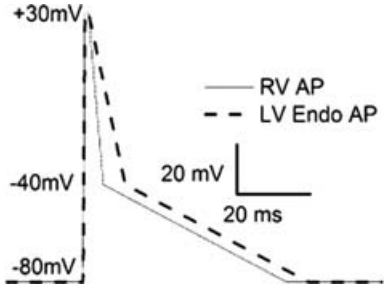

Figure 1. AP-like waveforms used for AP voltage-clamp experiments
These RV and LV endocardial AP-like waveforms were used for AP clamp experiments for both recording Ca^{2+} currents and myocyte shortening. The resting potential was −80 mV, the peak depolarization was +30 mV and the duration to the end of early repolarization (−40 mV) was 4 ms (RV) and 10 ms (LV endo). The durations were based on the primary data on mouse ventricle APD by Knollmann *et al.* (2001).

were analysed at steady state (reached within one to five AP command waveforms). In these experiments, series resistance was 1.4 ± 0.6 MΩ (RV) and 1.4 ± 0.6 MΩ (LV endo). The inward currents were blocked completely by Cd^{2+} (300 μM $CdCl_2$) which confirms that they were L-type Ca^{2+} currents (Linz & Meyer, 1998). Following leak subtraction, the inward current was averaged during the steady-state response to AP-controlled voltage clamps. This leak-subtracted inward current was compared to the inward current computed as the difference current before and after Cd^{2+} application (Fig. 2). Both were similar in seven different myocytes. Leak-subtracted currents were used for data analysis. All currents were normalized to whole-cell capacitance to allow these data to be expressed as peak current densities.

In these experiments, voltage clamped myocytes were imaged using a rapid scan (240 Hz) CCD camera (Philips) attached to an inverted microscope (Nikon Diaphot). The motion of the myocyte edges was tracked by a video edge detector (Crescent Electronics, Salt Lake City, UT, USA) and its voltage output was proportional to the change in myocyte length.

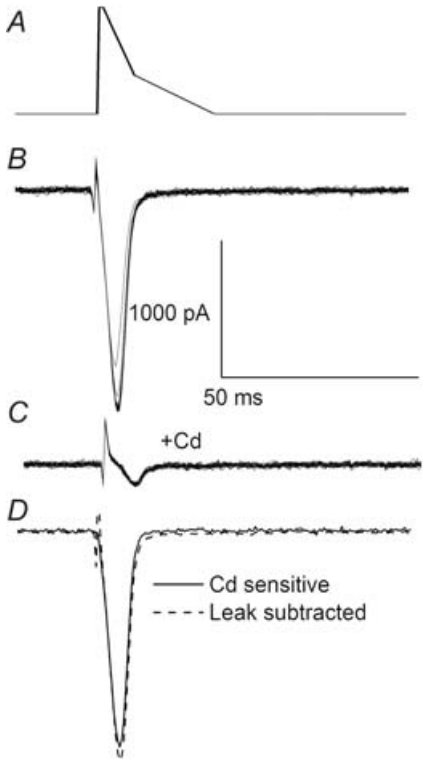

Figure 2. Isolation of the AP-triggered Ca^{2+} current
A, LV endocardial AP waveform used for AP-controlled voltage clamp. *B*, superimposed traces of inward currents recorded during LV endocardial AP clamp applied at 2 Hz. Steady-state currents were reached within four applied clamps. *C*, after the addition of 300 μM $CdCl_2$, inward currents were blocked, demonstrating that the inward current was the L-type Ca^{2+} current. *D*, following leak subtraction, the inward current was averaged during the steady-state response to AP-controlled voltage clamps. The leak-subtracted inward current was similar to the inward current computed as the difference current before and after Cd^{2+} application (and were similar in seven other myocytes). Therefore leak-subtracted currents were used for the data analysis.

Measurements of SR $^{45}Ca^{2+}$ uptake

RV free wall and LV subendocardial tissue from C57B6 8- to 10-week-old mouse hearts were homogenized at 4°C in 2.5 ml buffer solution (25 mM imidazole, pH 7.0) using a Teflon glass Thomas tissue grinder. SR $^{45}Ca^{2+}$ uptake assays were performed in those ventricular homogenates at room temperature using a protocol modified from that of Pagani & Solaro (1984). Aliquots (350 μl) of homogenates were transferred into tubes containing 2.8 ml experimental solution containing (mM): KCl 100, potassium oxalate 10, imidazole 40, sodium azide 10 and $MgCl_2$ 4 plus 1 μM ruthenium red, and $^{45}Ca^{2+}$–EGTA buffer containing 0.185 μCi ml^{-1} $^{45}Ca^{2+}$ (Perkin Elmer) and a preselected [Ca^{2+}] (20 and 200 nM), which was calculated on the basis of the amount of added EGTA. Ruthenium red was used to block $^{45}Ca^{2+}$ efflux from the sarcoplasmic reticulum via the ryanodine receptor. After 5-min preincubation, the Ca^{2+} uptake reaction was initiated by the addition of 2.5 mM sodium ATP. $^{45}Ca^{2+}$ uptake was terminated at selected times (1, 3 and 5 min for 200 nM [Ca^{2+}]; and 1, 10 and 20 min for 20 nM [Ca^{2+}]) by filtering 500-μl aliquots on 0.45-μm nitrocellulose membranes (Millipore-type MA), followed by two washes (5 ml) with uptake buffer without Ca^{2+} and ATP. The remaining radioactivity on the nitrocellulose filters was determined by liquid scintillation spectroscopy. Protein concentration was assayed with a DC protein assay kit (Bio-Rad). $^{45}Ca^{2+}$ uptake was calculated from the slope of the linear regression relating $^{45}Ca^{2+}$ uptake (mg protein)$^{-1}$ to reaction time.

Real-time PCR determination of Ca^{2+}-handling genes

Quantitative RT-PCR was performed to determine the relative mRNA expression pattern of the SR Ca^{2+} pump (SERCA2a), phospholambam (PLN), the predominant cardiac isoform of the Na^+–Ca^{2+} exchanger (NCX1), cardiac ryanodine receptor (RyR2) and cardiac L-type Ca^{2+} channel (Cav1.2) in the RV, LV subepicardium and LV subendocardium. RV, LV subepicardial and LV subendocardial tissue was manually dissected and pooled from three hearts of adult C57B6 male mice for each RNA isolation. Total RNA was extracted using the Trizol reagent (Gibco-BRL) and purified to remove any contaminating genomic DNA by on-column DNase digestion (Qiagen). First-strand synthesis and real-time amplification were performed using the Platinum qRT-PCR ThermoScript One-Step System (Invitrogene) with and the TaqMan Assays-on-Demand primer/probes pairs specific for GAPDH (Mm99999915_g1), cardiac

SERCA (Mm00437634_m1), RyR2 (Mm00465877_m1), PLN (Mm00452263_m1), NCX1 (Mm00444524–1) and Cav1.2 (Mm00437917_m1) (Applied Biosystems). Standard amplification curves were generated from GAPDH and the target genes with 320, 80 and 20 ng total RNA. Optimal PCR curves were observed within 40 cycles using the Mx4000 Multiplex Quantitative PCR System (Stratagene). Three sets of RNA isolations were evaluated and each measurement was performed in triplicate. The threshold value (C_t) was set with the amplification-based threshold algorithms from Stratagene. GAPDH expression of each sample was used as endogenous control. The fold-change expression differences of the target genes in 80 ng isolated RNA from the different locations (RV, LV endocardium and LV epicardium) were compared to the target gene expression in 80 ng whole-heart total RNA. Negative controls for possible contamination artefacts were performed, using Taq-Polymerase (Invitrogene) with the TaqMan primers/probes pairs, but without the reverse transcription step. These manoeuvres revealed no product amplification.

Data analysis

A two-way analysis of variance (ANOVA) with repeated measures was done to determine whether there were overall differences in the sarcomere shortening data at the three stimulation frequencies in the myocytes from RV, LV epicardium and LV endocardium. If an overall difference ($P < 0.05$, overall F statistic) was detected, one-way ANOVA was performed to compare RV, LV epicardium and LV endocardium at each individual stimulation frequency. Similarly, to analyse the frequency dependence of sarcomere shortening of myocytes from each tissue, one-way ANOVA with repeated measures was performed to compare the sarcomere shortening data at all three stimulation frequencies for each region. When the P-value for the overall F statistic for the one-way ANOVA was less than 0.05, *post hoc* Bonferroni tests were performed to assess the statistical significance ($P < 0.05$) for differences between the individual groups. When comparing two groups, paired t tests were used and $P < 0.05$ was considered significant. Data are expressed as mean ± S.E.M.

Results

Sarcomere shortening in RV and LV epicardium and endocardium

To assess whether there may be interventricular and/or regional differences in the unloaded shortening of isolated myocytes, sarcomere shortening in response to steady-state field stimulation was analysed in a large number of individual myocytes isolated from RV, LV subepicardium and LV subendocardium. Each myocyte was paced at three selected frequencies: 0.5, 1 and 2 Hz. In each case, measurements of sarcomere length were made at steady state and in Tyrode solution containing 1.0 mM $CaCl_2$. Figure 3*A* illustrates a typical experimental record from an RV myocyte and an LV endo myocyte. Figure 3*B* shows superimposed traces that were averaged over several beats ($n = 5$–15) during steady-state pacing of RV, LV subepicardial and LV subendocardial myocytes. Note that maximal sarcomere shortening in RV myocytes is significantly less than in myocytes from the LV endocardium from the same hearts at 0.5, 1 and 2 Hz. Additionally, a small but consistent difference at 2 Hz was observed between LV subepicardial myocytes and subendocardial myocytes (Figs 3*B* and 3*C*, and Table 1).

A related index of the phasic contraction of unloaded myocytes is the maximal velocity of shortening (Brady, 1991). Our analysis revealed that the maximal shortening velocity was significantly less in the RV myocytes than in LV myocytes (at 2 Hz: RV, $0.61 \pm 0.07\ \mu m\ s^{-1}$; LVepi, $0.88 \pm 0.1\ \mu m\ s^{-1}$; LVendo, $0.97 \pm 0.095\ \mu m\ s^{-1}$; $P < 0.05$).

The steepness of the relation between frequency and maximum unloaded sarcomere shortening also differed between RV, LV epicardial and LV endocardial myocytes. Increasing stimulation frequency decreased maximal sarcomere shortening in RV myocytes (Fig. 3). In contrast between 1 and 2 Hz, this relationship between sarcomere shortening and stimulation frequency was flat for LV endocardial myocytes (Fig. 3).

It is well known that sarcomere length can influence the development of force generation (Katz, 2001) and this has been demonstrated in ventricular trabeculae from mouse heart (Stuyvers *et al.* 2002). Accordingly, diastolic sarcomere length for each group of myocytes was assessed. However, there were no significant differences in resting sarcomere length in the myocytes from the three regions (Table 1).

To further evaluate support the previous pattern of results, additional experiments were done at $[Ca^{2+}]_o$ of 1.8 mM. Again, as expected, the contractions were significantly smaller in RV myocytes compared to LV endocardial myocytes (RV, $0.045 \pm 0.005\ \mu m$, $n = 74$; LVepi, $0.081 \pm 0.008\ \mu m$, $n = 84$; LVendo, $0.088 \pm 0.008\ \mu m$, $n = 75$; ANOVA RV *versus* LVepi, $P < 0.001$; and RV *versus* LVendo, $P < 0.001$).

$[Ca^{2+}]_i$ transients in RV and LV endocardial myocytes

To determine whether the interventricular and regional differences in sarcomere shortening were due to differences in $[Ca^{2+}]_i$, $[Ca^{2+}]_i$ transients were recorded in individual myocytes isolated from the RV and the LV subendocardium from the same hearts. $[Ca^{2+}]_i$ was

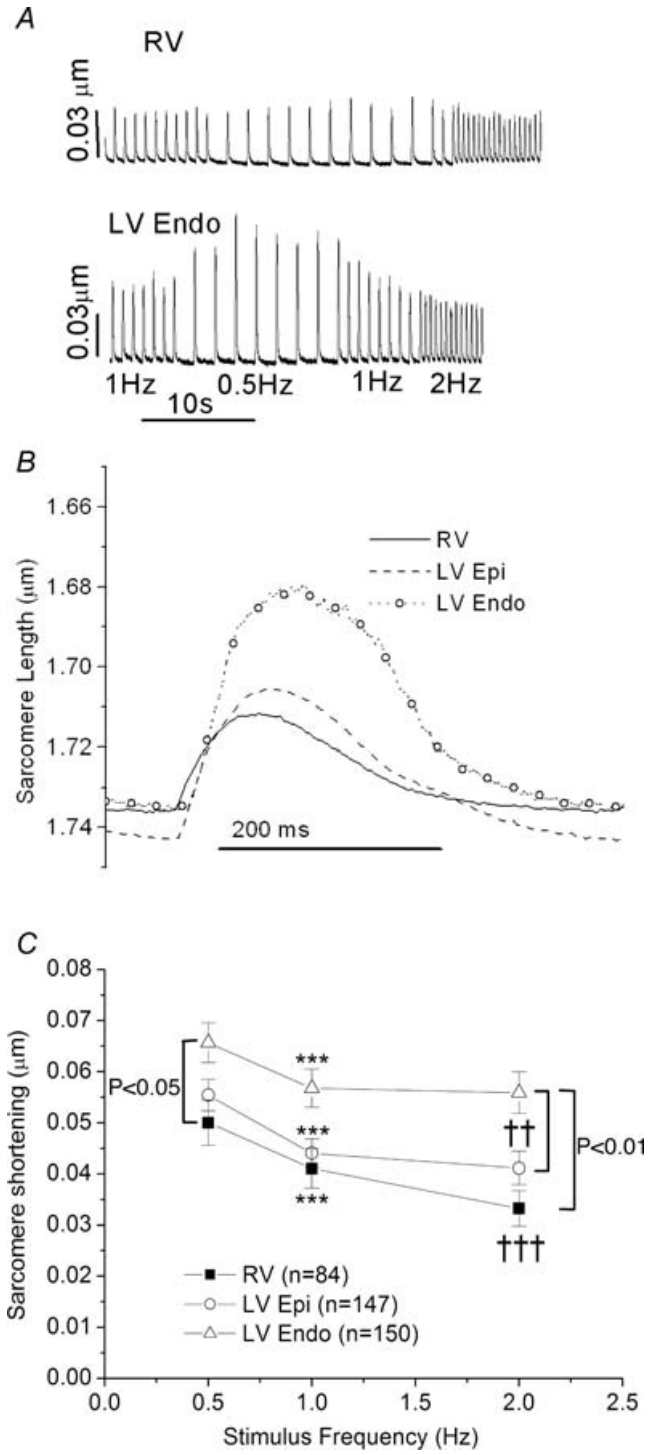

Figure 3. Region-specific differences in sarcomere shortening in ventricular myocytes from adult mouse hearts
A, a typical sarcomere shortening record from RV (top trace) and LV Endo (bottom trace). Both myocytes were paced in a sequence of 1, 0.5, 1 and 2 Hz and data were analysed at steady state. Calibration bars: vertical, 0.3 μm; horizontal, 10 s. *B*, records of sarcomere shortening averaged over 5–15 beats within the train of steady-state contractions. Each trace is a typical example from RV, LV subepicardium and LV subendocardium. *C*, plot of maximal sarcomere shortening at the pacing frequencies of 0.5, 1 and 2 Hz. Statistical analysis revealed significant differences between RV, LV epicardium and LV endocardium (two-way ANOVA with repeated measures; $P < 0.001$). Testing at each stimulation frequency showed that RV shortening ($n = 84$) was significantly less than LV subepicardial shortening ($n = 147$) at 2 Hz ($P < 0.01$) and LV subendocardial shortening ($n = 150$) at 0.5 Hz ($P < 0.05$), 1 Hz ($P < 0.01$) and 2 Hz ($P < 0.01$). Additionally, there was a significant decrease in sarcomere shortening in response to increases in stimulation frequency (***$P < 0.001$, 0.5 Hz *versus* 1 Hz and ††$P < 0.01$ 1 Hz *versus* 2 Hz, †††$P < 0.001$ 1 Hz *versus* 2 Hz). Temperature, 21°C.

monitored using Fura-4F, a Ca^{2+}-sensitive fluorescence indicator. In these experiments, the myocytes were paced at 0.5, 1 and 2 Hz; and all $[Ca^{2+}]_i$ transient measurements were made at steady state. To account for the expected Ca buffering by Fura-4F, the extracellular $[Ca^{2+}]$ was increased to 1.8 mM. Figure 4*A* shows typical experimental records (averaged over several beats, $n = 5$–15) from RV and LV subendocardial cells. Each $[Ca^{2+}]_i$ transient was analysed in terms of its baseline value and the height of the transient. Note that the amplitude of the Ca^{2+} transient is significantly larger in the LV subendocardial myocytes than in the RV myocytes (Fig. 4*B*) at 1 and 2 Hz. There were no differences in diastolic $[Ca^{2+}]_i$ (RV, 150 ± 30 nM; LVendo, 177 ± 18 nM). In agreement with the data in Fig. 3, maximum sarcomere shortening was greater in LV endocardial myocytes than in RV myocytes (at 2 Hz: RV, 0.032 ± 0.005 μm; LVendo, 0.0516 ± 0.009 μm, $P = 0.05$, *t* test) in this set of experiments.

K^+ current density in RV and LV epicardial and endocardial myocytes

The early phase of repolarization of the ventricular AP in mouse heart is more rapid in the RV compared to the LV (Knollmann *et al.* 2001) The APD is also shorter in LV epicardial myocytes compared to LV endocardial myocytes (Brunet *et al.* 2004). These differences are caused mainly by larger outward repolarizing K^+ currents in the RV and in the LV epicardium. In myocytes from adult mouse ventricle, the repolarizing K^+ currents at depolarized membrane potentials, consist of I_{to} and I_{Kur} (Fiset *et al.* 1997; Xu *et al.* 1999; Brouillette *et al.* 2004). We first sought to confirm that the K^+ current activated by depolarization differed in RV, LV epicardial and LV endocardial myocytes from adult mouse heart. Figure 5*A* illustrates typical examples of K^+ currents recorded during voltage-clamp step depolarization between −50 mV and +30 mV from an HP of −80 mV in RV, LV epicardial and LV endocardial myocytes. The current–voltage (*I–V*) relation of peak current density was approximately linear above the threshold voltage (Fig. 5*B*). When evaluated in terms of slope conductance (−10 mV to +30 mV) peak K^+ current density was significantly larger in RV myocytes compared to LV

Table 1. Myocyte shortening parameters in response to 2-Hz pacing

Parameter	RV	LV Epi	LV Endo
Baseline SL(μm)	1.738 ± 0.009 (6,84)	1.744 ± 0.005 (8147)	1.73 ± 0.005 (8150)
SL shortening (μm)	0.033 ± 0.003**,‡‡	0.041 ± 0.003††	0.056 ± 0.004
Rise time (50% to peak, ms)	54.7 ± 1	51 ± 1	54.7 ± 1
Decay time (50% to baseline, ms)	117 ± 5**, ‡‡	103 ± 3	98 ± 3

Within parenthesis, the first number indicates the number of hearts, and the second number indicates the total number of cells that have been studied. One-way ANOVA overall group difference $P < 0.01$. Pairwise comparisons: RV (**$P < 0.01$) and LVepi (††$P < 0.01$) different from LVendo; RV (‡‡$P < 0.01$) different from LVepi.

endocardial myocytes (RV, $1.31 \pm 0.15\ pA^{-1}\ pF^{-1}\ mV^{-1}$; LV Endo, $0.37 \pm 0.05\ pA^{-1}\ pF^{-1}\ mV^{-1}$, $P < 0.05$ ANOVA). This slope conductance was significantly larger in LV epicardial myocytes compared to LV endocardial myocyte (LV Epi, $1.0 \pm 0.16\ pA^{-1}\ pF^{-1}\ mV^{-1}$; LV Endo, $0.37 \pm 0.05\ pA^{-1}\ pF^{-1}\ mV^{-}1$, $P < 0.05$ ANOVA).

At membrane potentials near the resting potential, the inward rectifier K^+ current (I_{K1}) constitutes a significant repolarizing K^+ current in mouse ventricle. I_{K1} was recorded by applying, 500-ms steps between −120 mV to −40 mV from an HP of −80 mV. Figure 5*C* shows the *I–V* plot of I_{K1} density from RV, LV epicardial and LV endocardial myocytes. Note that there were no interventricular and transmural differences in I_{K1} density (Fig. 5*C*).

Ca^{2+} current density in RV and LV endocardial myocytes

As noted, the very brief AP plateau in mouse ventricular myocytes is modulated in part by the L-type Ca^{2+} current. This Ca^{2+} influx triggers phasic contraction. In principle, a larger calcium current could account for the greater sarcomere shortening in LV myocytes. Therefore, we compared L-type Ca^{2+} currents in RV and LV endocardial myocytes because these populations of myocytes show the greatest difference in APD and unloaded shortening. A HP of −40 mV was used to inactivate the Na current. To block K^+ currents, intracellular KCl was replaced isotonically by CsCl; TEA was added to the intracellular and extracellular solution and 2.5 mM 4-aminopyridine (4-AP) was added to the extracellular solution. L-type Ca^{2+} currents were recorded in RV and LV endocardial myocytes using rectangular depolarizing voltage-clamp steps between −50 mV and +45 mV from an HP of −40 mV. As shown in Fig. 6, there were no statistically significant differences in the *I–V* relation of peak Ca^{2+} current density between RV and LV endocardial myocytes (Fig. 6; $P = 0.11$ by *t* test, RV *versus* LVendo at $V_m = 0$).

Does the rate of repolarization during the AP modulate the Ca^{2+} current in mouse ventricle?

The duration of the early phase of repolarization of the mouse AP is similar to that of the L-type Ca^{2+} current.

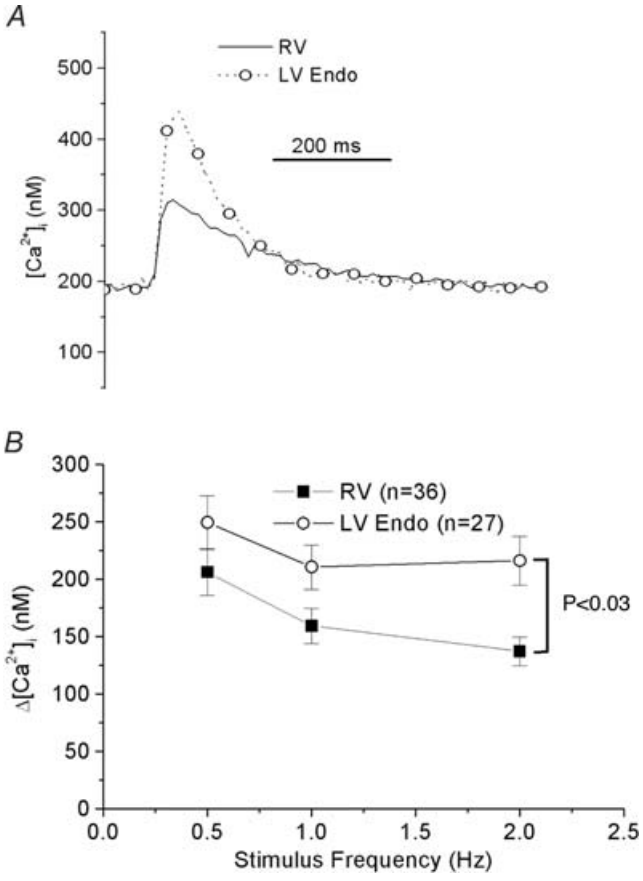

Figure 4. Region-specific differences in $[Ca^{2+}]_i$ transients in ventricular myocytes from adult mouse hearts
A, typical $[Ca^{2+}]_i$ transients (averaged over 5–15 beats) recorded during steady-state contractions from RV and LV endocardial myocytes paced at 2 Hz with 2-ms stimuli. Calibration bar, 200 ms.
B, graph showing the height (systolic − diastolic) of the $[Ca^{2+}]_i$ transient in RV and LV endocardial myocytes at the pacing frequencies of 0.5, 1 and 2 Hz. The height of the $[Ca^{2+}]_i$ transient in RV myocytes was significantly larger than that in LV subendocardial myocytes ($P < 0.03$, two-way ANOVA with repeated measures).

Thus the AP waveform may be an important modulator of the amplitude and kinetics of the Ca^{2+} current. To determine whether sarcolemmal Ca^{2+} influx is different during the RV AP compared to the LV endocardial AP, Ca^{2+} currents were measured in voltage-clamp experiments in which a digitally synthesized waveform resembling the AP of the RV and the LV endocardium was used as the command waveform. Figure 1 shows the applied RV and LV endocardial waveforms. Note that the only significant difference is the rate of repolarization following the peak of the AP. The same superfustate and Cs-based pipette solution were used as in the experiments shown in Fig. 6 except that 30 μM TTX was added to the extracellular solution to block the Na^+ current. The experimental protocol consisted of the application of 20 AP clamps having a selected waveform at 2 Hz frequency. Figure 7*A* shows typical steady-state recordings of Ca^{2+} current in an RV myocyte (left panel) and in an LV endocardial myocyte (right panel) (see Online Supplementary Material). To calculate the total Ca^{2+} influx during each such AP clamp waveform, the Ca^{2+} current was integrated. The integrals of the currents shown in Fig. 7*A* are plotted in Fig. 7*B*. Note that peak Ca^{2+} current was larger in response to RV AP

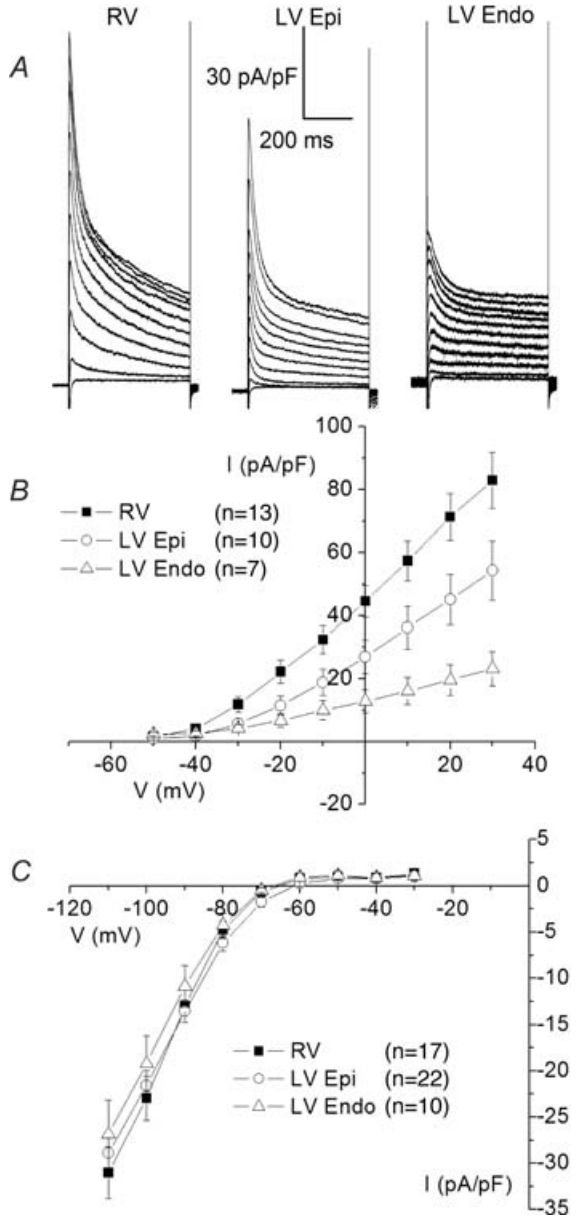

Figure 5. Region-specific differences in total outward K^+ current and inward rectifier K^+ current
A, superimposed traces of outward currents recorded in RV, LV epicardial and LV endocardial myocytes during a voltage-clamp protocol (HP, −80 mV; 500-ms depolarizing steps between −50 and +40 mV). Calibration bars apply for all three traces. The capacitance of the three myocytes was 70 pF (RV), 91 pF (LV Epi) and 49 pF (LV Endo), respectively. *B*, *I–V* plot of peak current density of K^+ current in RV, LV epicardial and LV endocardial myocytes. In terms of slope conductance of the respective *I–V* curves, RV and LV epicardial myocytes are significantly different from LV endocardial myocytes (see text). *C*, *I–V* relation of current density of the inward rectifier K^+ current (I_{K1}) recorded during 500 ms steps between −120 and −30 mV from an HP of −80 mV. There were no significant differences in I_{K1} between RV and LV myocytes.

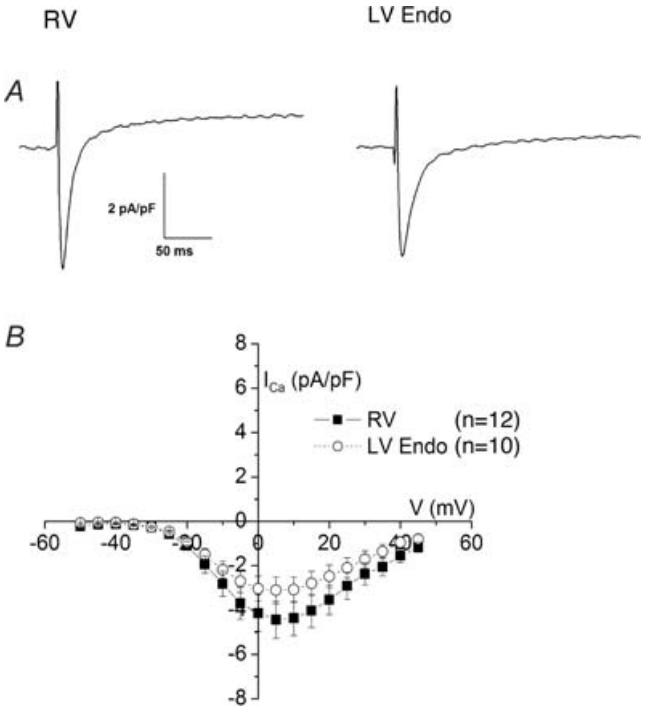

Figure 6. Lack of region-specific differences in the current–voltage relation of the L-type Ca^{2+} current
I–V plot of peak current density of $I_{Ca,L}$ in RV and LV endocardial myocytes. *A*, $I_{Ca,L}$ recorded during a voltage-clamp protocol using a depolarizing step for 500 ms to 0 mV from an HP of −40 mV. I_{Na} was inactivated by the HP of −40 mV and K^+ currents were blocked by isotonic replacement of K^+ by Cs^+, and the addition of 10 mM TEA and 2.5 mM 4-AP. The right panel shows a recording from an RV myocyte and the left panel illustrates a recording from an LV endocardial myocyte. *B*, the *I–V* relation of peak $I_{Ca,L}$ was determined by 500-ms depolarizing steps from −50 to +45 mV from an HP of −40 mV. There was no significant difference in the $I_{Ca,L}$ *I–V* relation between RV and LV endocardial myocytes.

compared to LV endocardial AP. This was true irrespective of myocyte origin (Fig. 7*C*). However, the integrated Ca^{2+} current was significantly larger in response to LV endocardial AP waveform, irrespective of the myocyte origin (Fig. 7*D*). Figure 7*E* shows the strong correlation between the integrated Ca^{2+} current for the RV AP and LV endocardial AP (RV myocytes, $R^2 = 0.95$; LV endocardial myocytes, $R^2 = 0.96$). The slope of the straight line fitted to this data was 1.20 ± 0.14 (RV myocytes) and 1.22 ± 0.1 (LV endocardial myocytes).

Does the rate of repolarization during the AP modulate myocyte shortening in mouse ventricle?

The larger total Ca^{2+} influx during the LV endocardial AP command waveform suggests that myocyte contraction could be modulated by the AP waveform. To assess whether changing the repolarization rate of the AP modulates myocyte contraction in mouse ventricle, myocyte shortening was measured during AP clamp. The extracellular solution was the same as that used for the experiments shown in Fig. 8. In these experiments, the pipette solution was to a standard K^+-based solution. This was considered to be necessary because K^+ serves as an effective counterion during SR Ca^{2+} release (Abramcheck & Best, 1989). In these studies, Ca^{2+} buffering in the pipette solution was reduced by the replacement of 5–10 mM EGTA, which is usually used in our voltage-clamp experiments, by 200 μM BAPTA. A sequence of 25 AP clamp was applied at waveform 2 Hz. Each protocol sequence was applied number of different times and the command waveform was altered between the RV AP and LV endocardial AP. To address the influence of a small rundown of myocyte shortening between protocols, the data for two successive RV AP protocol sequences were interpolated. This allowed more meaningful comparison of the intermediate data recorded using the LV endocardial waveform. Figure 8 shows representative current recordings (Fig. 8*A*) as well as the myocyte shortening records from the same myocytes (Fig. 8*B*). Note that the LV endocardial AP caused significantly larger myocyte shortening in both RV and LV endocardial myocytes than the RV waveform (Fig. 8*C*).

Sarcoplasmic reticulum Ca^{2+}-ATPase activity

To determine whether the larger $[Ca^{2+}]_i$ transient in LV myocytes could be due to an intrinsically greater SR Ca^{2+}-ATPase activity in these myocytes, SR Ca^{2+}-ATPase activity was assessed in RV and LV endocardial tissue. A $^{45}Ca^{2+}$ flux assay was applied using SR vesicles prepared from RV and LV subendocardium (Pagani & Solaro, 1984). At the extravesicular $[Ca^{2+}]$ of 20 nM, $^{45}Ca^{2+}$ flux was 0.66 ± 0.2 (RV) and 1.1 ± 0.37 (LVendo) and at the extravesicular $[Ca^{2+}]$ concentration of 200 nM, $^{45}Ca^{2+}$ flux was 49.5 ± 2 (RV) and 44.7 ± 6 (LVendo). No statistically significant differences between RV and LV endocardium were found.

mRNA expression of Ca^{2+}-handing proteins in mouse ventricular myocytes

To assess whether there are interventricular differences in the expression levels of well-known Ca^{2+}-handling proteins in these myocytes, the relative mRNA transcript level of SERCA2a, PLN, RyR2, NCX1 and Cav1.2 were compared in RV, LV subepicardium and LV subendocardium using quantitative PCR. No differences in mRNA expression were identified (Fig. 9).

Can block of voltage-dependent K^+ currents modulate shortening in ventricular myocytes from adult mouse?

In myocytes from adult mouse ventricle, the depolarization-activated outward K^+ current is composed at least of two separate K^+ conductances, I_{to} and I_{Kur}. These K^+ currents have different voltage ranges for activation and inactivation and also exhibit different kinetics of inactivation (Xu *et al.* 1999; Brouillette *et al.* 2004). Both K^+ currents are blocked by 4-AP (Josephson *et al.* 1984; Brouillette *et al.* 2004). I_{Kur} is strongly inhibited by 50–100 μM 4-AP (Fiset *et al.* 1997), while I_{to} is blocked by concentrations of 2–5 mM 4-AP (Brouillette *et al.* 2004). 4-AP (100 μM) markedly slows the rate of early repolarization and broadens the AP at both early and later phases (Brouillette *et al.* 2004) by blocking I_{Kur}.

To test whether the block of K^+ currents can affect unloaded shortening in mouse ventricular myocytes, sarcomere shortening was recorded in RV, LV epicardial and LV endocardial myocytes exposed to 100 μM 4-AP which blocks I_{Kur}. The $[Ca^{2+}]_o$ was 1 mM in these experiments as in the initial studies, (Fig. 3). In all experiments, 100 μM 4-AP increased maximal sarcomere shortening in RV, LV epicardial and LV endocardial myocytes compared to the maximal sarcomere shortening at the same stimulus frequencies in the absence of 4-AP (Fig. 10). However, even with 100 μM 4-AP present, sarcomere shortening in RV myocytes was smaller than in LV subendocardial myocytes. Increasing the stimulation frequency from 0.5 to 1 and 2 Hz, decreased sarcomere shortening for RV myocytes ($P < 0.001$). This also appeared to be the case for LV epicardial myocytes although the small difference failed to reach statistical significance ($P = 0.06$). In contrast, the shortening versus frequency relationship was flat for LV endocardial myocytes.

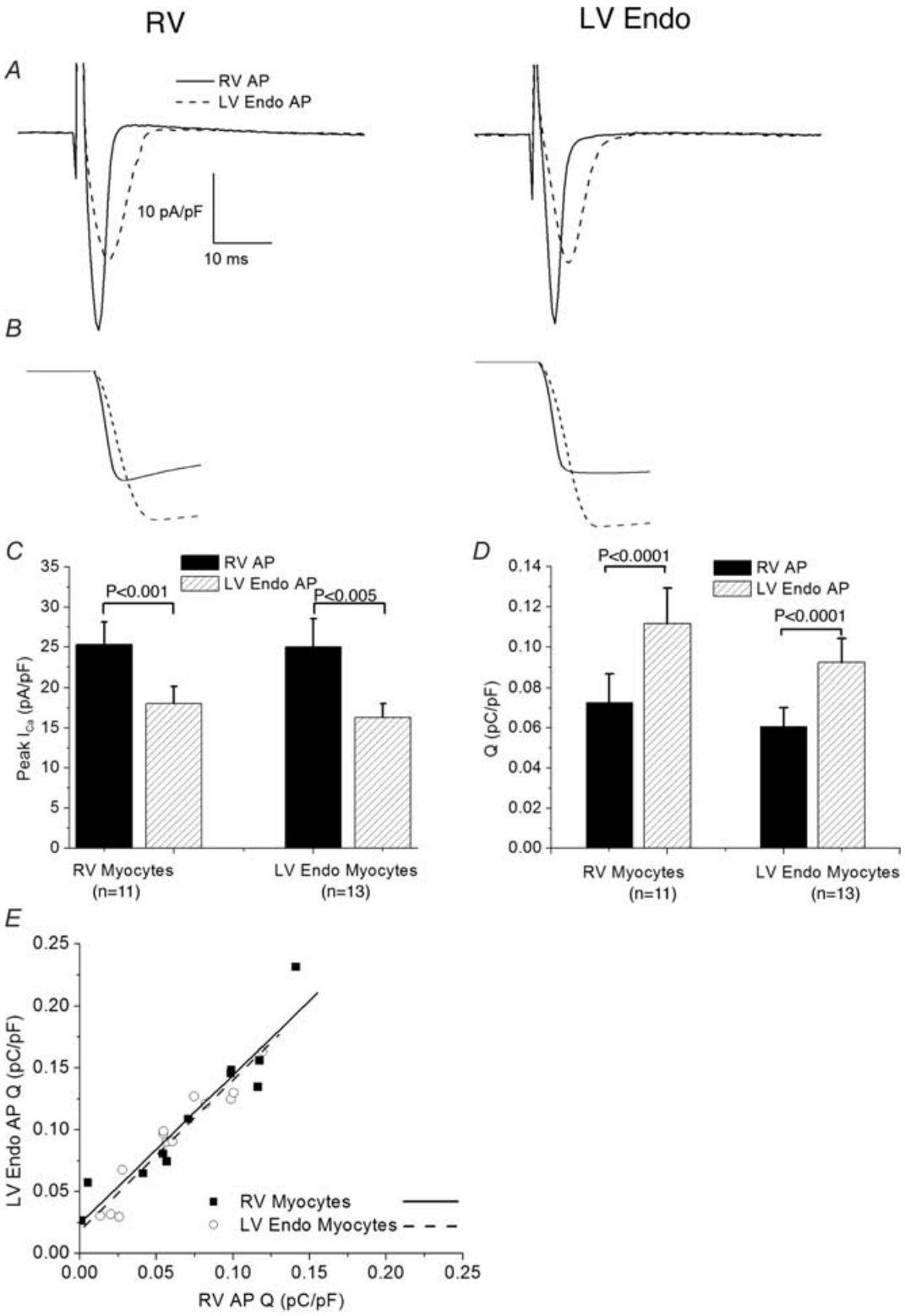

Figure 7. Ca^{2+} currents elicited by RV and LV endocardial AP clamp in myocytes from RV or LV endocardium

A, Ca^{2+} currents recorded during an RV AP (solid line) and LV endocardial AP (dashed line) in an RV myocyte (left panel) and an LV endocardial myocyte (right panel). Sequences of either 20 RV AP clamp waveforms or 20 LV endocardial AP clamp waveforms were applied at 2 Hz. Following leak-subtraction, the inward current was averaged over the train of steady-state current recordings. I_{Na} was blocked by 30 μM TTX and K^+ currents were blocked by isotonic replacement of K^+ by Cs^+, and addition of 10 mM TEA and 2.5 mM 4-AP (see Methods).

Millimolar levels of 4-AP would be required to block both I_{to} and I_{Kur}. However, experiments could not be done in the presence of 3–5 mM 4-AP; many myocytes exhibited rapid, spontaneous contractions. This precluded meaningful measurements of resting sarcomere length and field-stimulated phasic contractions (data not shown).

Discussion

Summary of main findings

The present study demonstrates large and consistent differences in sarcomere shortening between unloaded myocytes isolated from RV and LV myocardium of the adult mouse heart. These differences in maximal shortening are both interventricular and transmural as demonstrated by the significant differences in sarcomere shortening of myocytes from LV subepicardium and LV subendocardium. The transmural difference in sarcomere shortening is consistent with a somewhat similar 'mechanical gradient' described for myocytes isolated from dog LV epicardium and endocardium (Cordeiro *et al.* 2004). Our data (Fig. 3) show that whether assessed in terms of maximal contraction or by maximal shortening velocity, unloaded shortening of myocytes from RV is less than that of LV myocytes. In addition, unloaded shortening of LV epicardial myocytes is less than that of LV endocardial myocytes. $[Ca^{2+}]_i$ measurements reveal corresponding differences in $[Ca^{2+}]_i$ transients between RV and LV endocardial myocytes. In particular, the peak values of $[Ca^{2+}]_i$ are significantly larger in LV endocardial myocytes. These results suggest that different $[Ca^{2+}]_i$ dynamics in RV, LV epicardium and LV endocardium are an important factor which can regulate the differences in unloaded myocyte shortening that were observed in these tissues.

Difference from previously reported results with cat myocytes

It should be noted that in cat, no differences in contractile properties were observed between RV and LV myocytes (Kleiman & Houser, 1988). It is interesting that in this same study, no differences in APD between RV and LV were identified. On the other hand in studies of rat, the force generation of RV papillary muscle was less than that of LV papillary muscle and the shortening velocity of isolated RV myocytes was less than that of LV myocytes (Brooks *et al.* 1987; Harding *et al.* 1990). LV transmuted that electrophysiological differences are manifest in mouse (Brunet *et al.* 2004), rat (Casis *et al.* 1998) and dog (Di Diego *et al.* 1996; Antzelevitch & Dumaine, 2001) and that these differences may play a role in chamber-specific myocyte contractile properties, the results from cat may reflect a species-specific phenotype.

Regional differences in cardiac electrophysiology in mouse ventricle

Shorter APD in the RV relative to LV as well as shorter APD in LV epicardium relative to LV endocardium have been identified in studies in a number of different mammalian ventricles (Clark *et al.* 1993; Di Diego *et al.* 1996; Knollmann *et al.* 2001). In general, this pattern of APD differences correlates with a similar pattern of K^+ current density (RV > LV and LV epi > LV endo)(Clark *et al.* 1993; Di Diego *et al.* 1996; Brunet *et al.* 2004). In contrast, we did not observe a statistically significant difference in the *I–V* relation of $I_{Ca,L}$ peak current density of RV vs LV myocytes. Thus, our data do not support the hypothesis that a reduced $I_{Ca,L}$ density is responsible for the shorter RV APD. Furthermore, the lack of regional differences in the mRNA transcript level of Cav1.2, the α-subunit of the L-type Ca^{2+} channel (Fig. 9), is consistent with the conclusion that a reduction in Cav1.2 in the RV is not responsible for the shorter RV APD.

Effect of AP waveform on Ca^{2+} currents and myocyte shortening

The initial repolarization rate as well as AP height and duration are important inotropic factors (Wood *et al.* 1969; Allen, 1977). As shown in our previous AP-controlled voltage-clamp study in rat ventricular myocytes, slowing the rate of the initial repolarization of the AP increased the total amount of Ca^{2+} entry per AP waveform and also increased maximal myocyte shortening (Bouchard *et al.* 1995). The larger total Ca^{2+} entry per AP myocytes provide a larger

B, the integral of the inward Ca^{2+} current from *A*. *C*, mean peak Ca^{2+} current density recorded during AP clamp. Note that the peak current recorded during LV endocardial AP clamp was significantly smaller (compared using paired *t* test) than during RV AP clamp for both RV myocytes and LV endocardial myocytes. There was no difference in peak Ca^{2+} current between RV and LV endocardial myocytes. *D*, mean integral of the Ca^{2+} current (total charge, *Q*) entering the myocyte, expressed in terms of myocyte capacitance. Total charge entering both RV and LV endocardial myocytes is significantly greater with the LV endocardial AP waveform than with the RV AP voltage-clamp waveform. *E*, the correlation between the total charge entry during an RV AP compared to during an LV endocardial AP. The solid line shows the linear regression fit for RV myocytes and the dashed line is the fit for LV endocardial myocytes. Note that the correlation is very similar for both myocyte populations. The slope of the lines are 1.2 ± 0.14 (RV myocytes) and 1.22 ± 0.1 (LV endo myocytes). F. Confirmation of the recording of a

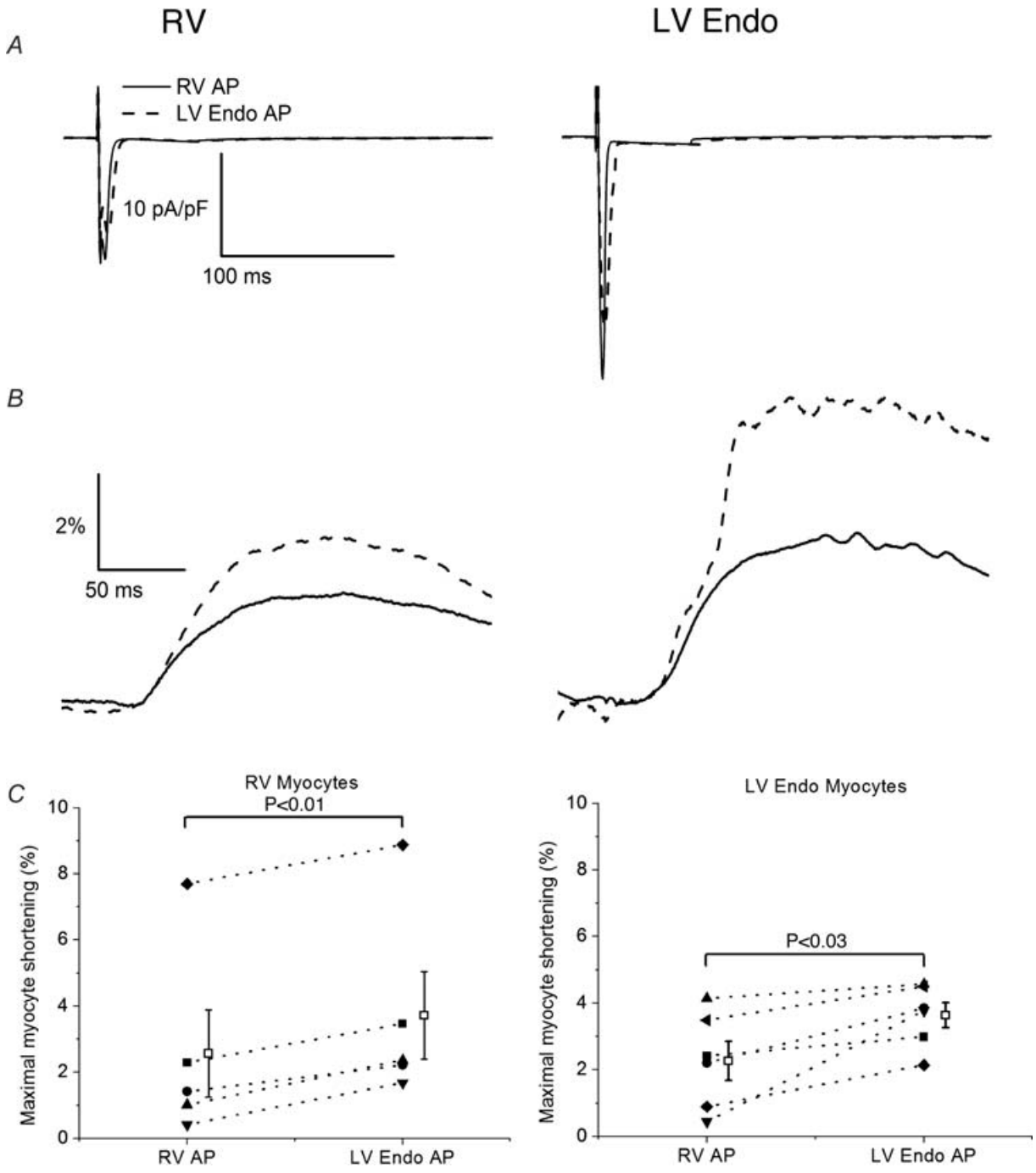

Figure 8. Unloaded myocyte shortening in RV and LV endocardial myocytes due to applied RV and LV endocardial AP voltage clamp waveform

A, Ca^{2+} currents recorded using an RV AP waveform (solid line) and LV endocardial AP waveform (dashed line) in an RV myocyte (left panel) and an LV endocardial myocyte (right panel). The experimental protocol was the same as in Fig. 6 except that the stimulation sequence consisted of 25 AP clamps at 2 Hz. *B*, record of average myocyte shortening at steady state (determined from the shortening data). Contractions were triggered by the sequence of AP clamps from the same myocytes from which Ca^{2+} currents were recorded for panel *A*. The solid line shows shortening in response to the RV AP and the dashed line shows shortening in response to the LV endocardial AP. *C*, scatter plot of myocyte shortening due to RV AP and LV endocardial AP waveforms in individual myocytes. The connecting broken lines indicate the effect of switching AP waveform on the same myocyte. The open boxes with error bars show the mean data with S.E.M. Note that myocyte shortening was significantly greater with the LV endocardial AP than with the RV AP (paired *t* test) in both RV (left panel) and LV endocardial myocytes (right panel).

trigger for SR Ca^{2+} release. If it persists (e.g. APD are prolonged for a substantial time period), the Ca^{2+} influx results in enhanced SR Ca^{2+} loading and increased SR Ca^{2+} content. The evidence provided by Bouchard *et al.* (1997) suggests that slowing repolarization has a modest effect on the Ca^{2+} trigger for SR release but a greater effect on SR Ca^{2+} loading in rat ventricular myocytes.

This finding and subsequent results by others (Sah *et al.* 2003) suggests the possibility that the slower repolarization of the LV endocardial AP might contribute to the larger sarcomere shortening in LV endocardial myocytes. Figures 7 and 8 confirm that slowing repolarization can increase. The total influx of Ca^{2+} and myocyte shortening in mouse ventricular myocytes. These results also show that the quantitative effect of AP waveform on Ca^{2+} entry and myocyte shortening is independent of the anatomical origin of the myocyte. Thus the data strongly suggest that the regional differences in AP waveform, and in repolarization rate in particular, are critical for explaining the regional differences in myocyte contraction and Ca^{2+} handling.

We did not directly explore the mechanisms underlying the transmural differences in sarcomere shortening in the LV. However, given the similar, albeit smaller in magnitude, differences in outward K^+ current density (Fig. 5) and APD (Knollmann *et al.* 2001), a similar pattern of differences would be expected. Previous work using AP-controlled voltage clamp with rat ventricular myocytes, has shown that switching the voltage clamp from an epicardial-like AP to an endocardial-like AP in the same ventricular myocyte significantly increased the amount of Ca^{2+} entry (Volk & Ehmke, 2002).

Other potential mechanisms causing regional differences in myocyte shortening

Despite the consistent difference in $[Ca^{2+}]_i$ transients between RV and LV myocytes, our measurements of $^{45}Ca^{2+}$ uptake in SR vesicles isolated from RV and LV endocardial tissue homogenates demonstrate that there is no measurable difference in intrinsic SR Ca^{2+} pump activity between RV and LV (Fig. 7). A quantitative PCR analysis failed to reveal any differences in the mRNA transcript levels of five important Ca^{2+} handling proteins (SERCA2a, phospholambam, NCX1, RYR2 and Cav1.2) (Fig. 9). However, our results do not exclude the possibility of other differences in Ca^{2+} handling in addition to the mechanism we have studied. A more complete analysis would require an assessment of the protein levels of the components of the Ca^{2+}-handling system, including their phosphorylation state and changes in the setting of adrenergic signalling in RV, LV epicardium and LV endocardium. Furthermore, the AP waveform-dependent mechanism operates on a rapid time scale (several beats), while changes in the phosphorylation state of Ca^{2+}-handling proteins are likely to provide slower, longer-term regulation of the contractile state. Thus, our AP waveforms differences can produce regional conclusion that variations of myocyte contraction

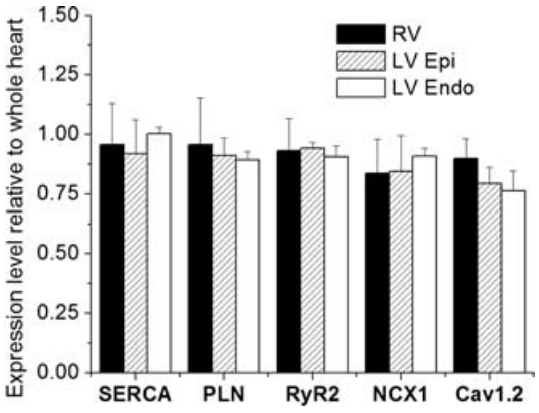

Figure 9. Quantitative PCR of gene expression major of Ca^{2+} handling proteins in mouse ventricle tissue
Comparison of mRNA levels of SERCA2a, PLB, RyR2, PLB and Cav1.2 in RV and LV endocardial tissue. The mRNA expression levels of these proteins and the reference that compound GAPDH in RV, LV epicardium, LV endocardium and whole heart, were quantified by real-time PCR. The mRNA levels of the Ca^{2+}-handling proteins were normalized relative to the GAPDH mRNA expression level. The expression level in RV, LV epicardium and LV endocardium were expressed as a ratio relative to the expression level in the whole heart. There were no observed differences between RV, LV epicardium and LV endocardium.

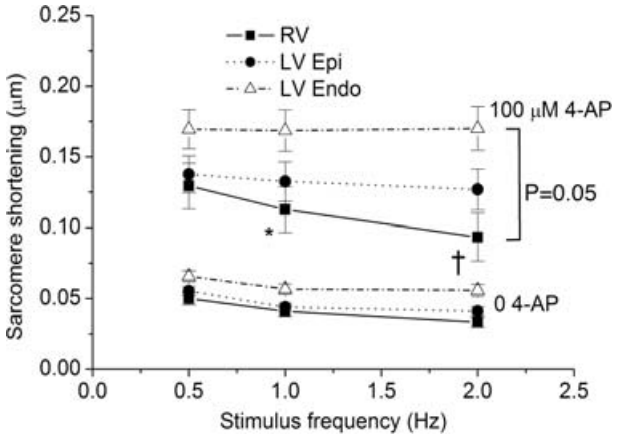

Figure 10. Sarcomere shortening in the presence of the K^+ current blocker, 100 μM 4-aminopyridine
Plot of maximal sarcomere shortening recorded during steady state at three different pacing frequencies of 0.5, 1 and 2 Hz in myocytes from RV, LV epicardium and LV endocardium. Also shown on this plot is the sarcomere shortening data from Fig. 3 without 4-AP for comparison. In the presence of 100 μM 4-AP, maximal sarcomere shortening for all three types of ventricular myocytes is significantly larger than without 4-AP. There were significant differences in sarcomere shortening between RV, LV epicardium and LV endocardium (two-way ANOVA with repeated measures, $P = 0.05$). Increasing stimulation frequency decreased sarcomere shortening for RV myocytes (*$P < 0.05$, 0.5Hz *versus* 1Hz and †$P < 0.05$ 1 Hz *versus* 2 Hz; one-way ANOVA with repeated measures).

could in parallel e.g. a mechanism involving could be modulated by differential phosphorylation.

Based on the findings on this study, we cannot exclude the possibility that there are region-specific differences in the Ca^{2+} sensitivity of the contractile proteins in the myofilaments. Therefore, it is possible that a lower Ca^{2+} sensitivity of the contractile proteins in the RV compared to the LV may contribute to an overall reduction in myocyte shortening in RV myocytes compared to LV myocytes.

Similarly, we cannot exclude the possibility that a specific feature of the experiments (e.g. temperature) contributed to this pattern of findings. In previous studies, APs have been measured in the RV epicardium, LV epicardium and LV endocardium of the intact mouse heart perfused at physiological temperatures (Knollmann *et al.* 2001). Regional differences of APD are present at all of these temperatures. The large current densities (Na^+ and K^+), which are characteristic of murine and rat myocytes, make it difficult if not impossible to ensure adequate voltage control in single-electrode, voltage-clamp experiments in these species at physiological temperatures (Bouchard *et al.* 1995; Clark, Bouchard and Giles, 1996). Accordingly, we have conducted the experiments at room temperature where difficulties with voltage control are reduced.

Effect of the block of K^+ currents on myocyte shortening

In our study, blocking one component of the time- and voltage-dependent K^+ current (I_{Kur} or *I*Kv1.5) with 100 μM 4-AP, increased unloaded sarcomere shortening (Fig. 10). This is consistent with our previous work in which 50 μM 4-AP increased the force of contraction in the isolated, working mouse heart (Fiset *et al.* 1997). In RV myocytes, 100 μM 4-AP has been shown to increase time from peak AP to 50% repolarization (APD_{50}) from 4 to 15 ms (Brouillette *et al.* 2004); thus, the mechanism of the 4-AP-induced inotropic effect is probably due to the effect of slowed repolarization and prolonged APD on net Ca^{2+} influx.

It is important to note that 100 μM 4-AP did not eliminate the regional differences in sarcomere shortening. It is possible that after the block of I_{Kur} (Kv1.5) there are still differences in AP repolarization between RV, LV epicardial and LV endocardial myocytes. However, we did not measure the effect of 100 μM 4-AP on APD_{50} in LV epicardial and LV endocardial myocytes.

Frequency dependence of sarcomere shortening

A change in the stimulation frequency causes a change in force generation by cardiac muscle (Blinks & Koch-Weser, 1961; Bers, 2001; Georgakopoulos & Kass, 2001; Stuyvers *et al.* 2002). In mouse ventricular myocytes, we observed a negative frequency dependence between the stimulation frequencies of 0.5 and 2 Hz at 19–21°C. In mouse ventricular myocytes, the relation between stimulation frequency and steady-state sarcomere shortening has been shown to be dependent on the balance between a decrease in $I_{Ca,L}$ with increasing stimulation frequencies, and an increase in SR Ca^{2+} loading at higher frequencies (Antoons *et al.* 2002). Our data suggest that this balance of Ca^{2+} entry and SR Ca^{2+} loading differs between ventricular myocytes from RV, LV epicardium and LV endocardium.

Physiological relevance of these results

Our findings are consistent with the previously identified relationship between K^+ current density, APD and myocyte shortening (Bouchard *et al.* 1995; Volk *et al.* 1999; Sah *et al.* 2003). Thus, sarcomere shortening was largest in LV endocardial myocytes where the K^+ current density is smallest (Brunet *et al.* 2004). In fact, sarcomere shortening varied approximately inversely with total outward K^+ current density and APD (Knollmann *et al.* 2001; Brunet *et al.* 2004) in mouse heart. In summary, our data suggest that regional differences of outward K^+ current density may play a role in modulating excitation–contraction coupling in addition to its established role in setting the gradient for early repolarization of the AP (Antzelevitch, 2001; Kuo *et al.* 2001; Costantini *et al.* 2005).

It should be noted that in the present study, the RV myocyte population was a mixture of RV epicardial and RV endocardial myocytes. The thin wall of the RV prevented an unambiguous separation of myocytes from these two regions. Transmural differences in repolarization across the RV wall have been reported (Knollmann *et al.* 2001); thus, it is probable that transmural differences exist in contractile properties of RV myocytes.

Contraction of the intact ventricular chamber involves a torsional twisting of the laminar architecture of the myocardial fibres (Costa *et al.* 1999). How a transmural gradient of contractile properties of LV myocytes contributes to this remains unknown. However, a recent simulation study has indicated that transmural heterogeneity of repolarization provides an electromechanical advantage in myocardial mechanics (Nickerson *et al.* 2005).

Limitations of this study

The known anatomical differences between the right and left mammalian ventricles present a significant limitation for detailed comparisons of contractility. These variations include differences in fibre orientation and muscle thickness. Thus, studies of force generation by ventricular trabeculae would be difficult to interpret given the differential fibre orientation and

muscle thickness in RV and LV. Isolated myocytes provide an opportunity to measure contractile characteristics from well-defined, reproducible sites in the myocardium. Another limitation of our approach uncertainly concerning is whether differences in unloaded shortening parameters measured at room temperature are a reliable index of *in vivo* contractility. This has not been addressed in this paper. Nonetheless, our results demonstrate substantial, consistent differences in contractile behaviour between RV and LV and provide new insights into the potential mechanisms responsible for distinct RV and LV pathophysiology in models of cardiac disease (Grattan *et al.* 2005). Finally, studies have identified different RV and LV diastolic filling patterns in mouse heart (Zhou *et al.* 2003) and revealed a significant role of preload in regulating murine cardiac contractility (Stull *et al.* 2002). Accordingly *in vivo*, the reduced unloaded shortening in RV myocytes may arise from the distinct pressure profiles of the right and left chambers of the mouse heart as well as intrinsic differences in APD.

References

Abramcheck CW & Best PM (1989). Physiological role and selectivity of the in situ potassium channel of the sarcoplasmic reticulum in skinned frog skeletal muscle fibers. *J Gen Physiol* **93**, 1–21.

Allen DG (1977). On the relationship between action potential duration and tension in cat papillary muscle. *Cardiovasc Res* **11**, 210–218.

Antoons G, Mubagwa K, Nevelsteen I & Sipido KR (2002). Mechanisms underlying the frequency dependence of contraction and $[Ca^{2+}]_i$ transients in mouse ventricular myocytes. *J Physiol* **543**, 889–898.

Antzelevitch C (2001). Molecular basis for the transmural distribution of the transient outward current. *J Physiol* **533**, 1.

Antzelevitch C Dumaine R (2001). Electrical heterogeneity in the heart: physiological, pharmacological and clinical implication. In page E, Forzzard HA, Solaro RJ, eds. *Handbook of Physiology*. New York: Oxford University Press, 654–692.

Barry WH & Bridge JH (1993). Intracellular calcium homeostasis in cardiac myocytes. *Circulation* **87**, 1806–1815.

Bassani RA, Altamirano J, Puglisi JL & Bers DM (2004). Action potential duration determines sarcoplasmic reticulum Ca^{2+} reloading in mammalian ventricular myocytes. *J Physiol* **559**, 593–609.

Bers DM (2001). *Excitation-Contraction Coupling and Cardiac Contractile Force*, 2nd edn, Kluwer Academic, Boston.

Blinks JR & Koch-Weser J (1961). Analysis of the effects of changes in rate and rhythm upon myocardial contractility. *J Pharmacol Exp Ther* **134**, 373–389.

Bouchard RA, Clark RB & Giles WR (1995). Effects of action potential duration on excitation-contraction coupling in rat ventricular myocytes. Action potential voltage-clamp measurements. *Circ Res* **76**, 790–801.

Brady AJ (1991). Mechanical properties of isolated cardiac myocytes. *Physiol Rev* **71**, 413–428.

Brooks WW, Bing OH, Blaustein AS & Allen PD (1987). Comparison of contractile state and myosin isozymes of rat right and left ventricular myocardium. *J Mol Cell Cardiol* **19**, 433–440.

Brouillette J, Clark RB, Giles WR & Fiset C (2004). Functional properties of K^+ currents in adult mouse ventricular myocytes. *J Physiol* **559**, 777–798.

Brouillette J, Trepanier-Boulay V & Fiset C (2003). Effect of androgen deficiency on mouse ventricular repolarization. *J Physiol* **546**, 403–413.

Brunet S, Aimond F, Li H, Guo W, Eldstrom J, Fedida D, Yamada KA & Nerbonne JM (2004). Heterogeneous expression of repolarizing, voltage-gated K^+ currents in adult mouse ventricles. *J Physiol* **559**, 103–120.

Casis O, Iriarte M, Gallego M & Sanchez-Chapula JA (1998). Differences in regional distribution of K^+ current densities in rat ventricle. *Life Sci* **63**, 391–400.

Clark RB, Bouchard RA & Giles WR (1996). Action potentiol duration modulates calcium influx $Na^+ - Ca^{2+}$ exchange, and intracellular calcium release in rat ventricular myocytes. *Annals of N. Y. Acad. Sci.* **779**, 417–429.

Clark RB, Bouchard RA, Salinas-Stefanon E, Sanchez-Chapula J & Giles WR (1993). Heterogeneity of action potential waveforms and potassium currents in rat ventricle. *Cardiovasc Res* **27**, 1795–1799.

Cordeiro JM, Greene L, Heilmann C, Antzelevitch D & Antzelevitch C (2004). Transmural heterogeneity of calcium activity and mechanical function in the canine left ventricle. *Am J Physiol Heart Circ Physiol* **286**, H1471–H1479.

Costa KD, Takayama Y, McCulloch AD & Covell JW (1999). Laminar fiber architecture and three-dimensional systolic mechanics in canine ventricular myocardium. *Am J Physiol* **276**, H595–H607.

Costantini DL, Arruda EP, Agarwal P, Kim KH, Zhu Y, Zhu W, *et al.* (2005). The homeodomain transcription factor Irx5 establishes the mouse cardiac ventricular repolarization gradient. *Cell* **123**, 347–358.

Di Diego JM, Sun ZQ & Antzelevitch C (1996). I_{to} and action potential notch are smaller in left vs. right canine ventricular epicardium. *Am J Physiol* **271**, H548–H561.

Fiset C, Clark RB, Larsen TS & Giles WR (1997). A rapidly activating sustained K^+ current modulates repolarization and excitation-contraction coupling in adult mouse ventricle. *J Physiol* **504**, 557–563.

Georgakopoulos D & Kass D (2001). Minimal force-frequency modulation of inotropy and relaxation of in situ murine heart. *J Physiol* **534**, 535–545.

Grattan MJ, Kondo C, Thurston J, Alakija P, Burke BJ, Stewart C, Syme D & Giles WR (2005). Skeletal and cardiac muscle defects in a murine model of Emery-Dreifuss muscular dystrophy. *Novartis Found Symp* **264**, 118–133.

Grynkiewicz G, Poenie M & Tsien RY (1985). A new generation of Ca^{2+} indicators with greatly improved fluorescence properties. *J Biol Chem* **260**, 3440–3450.

Harding SE, O'Gara P, Jones SM, Brown LA, Vescovo G & Poole-Wilson PA (1990). Species dependence of contraction velocity in single isolated cardiac myocytes. *Cardioscience* **1**, 49–53.

Josephson IR, Sanchez-Chapula J & Brown AM (1984). Early outward current in rat single ventricular cells. *Circ Res* **54**, 157–162.

Katz A (2001). *Physiology of the Heart*, 3rd edn, Lippincott, Williams & Wilkins, Philadephia.

Kleiman RB & Houser SR (1988). Electrophysiologic and mechanical properties of single feline RV and LV myocytes. *J Mol Cell Cardiol* **20**, 973–982.

Knollmann BC, Katchman AN & Franz MR (2001). Monophasic action potential recordings from intact mouse heart: validation, regional heterogeneity, and relation to refractoriness. *J Cardiovasc Electrophysiol* **12**, 1286–1294.

Kuo HC, Cheng CF, Clark RB, Lin JJ, Lin JL, Hoshijima M *et al.* (2001). A defect in the Kv channel-interacting protein 2 (KChIP2) gene leads to a complete loss of I_{to} and confers susceptibility to ventricular tachycardia. *Cell* **107**, 801–813.

Linz KW & Meyer R (1998). Control of L-type calcium current during the action potential of guinea-pig ventricular myocytes. *J Physiol* **513**, 425–442.

Nabauer M, Callewaert G, Cleemann L & Morad M (1989). Regulation of calcium release is gated by calcium current, not gating charge, in cardiac myocytes. *Science* **244**, 800–803.

Nickerson D, Smith N & Hunter P (2005). New developments in a strongly coupled cardiac electromechanical model. *Europace* **7** (Suppl. 2), 118–127.

Pagani ED & Solaro RJ (1984). Methods for measuring functional properties of sarcoplasmic reticulum and myofibrils in small samples of myocardium. In *Methods Pharmacol* ed. Schwartz A, pp. 49–61. Plenum Publishing, New York.

Rosati B, Grau F, Rodriguez S, Li H, Nerbonne JM & McKinnon D (2003). Concordant expression of KChIP2 mRNA, protein and transient outward current throughout the canine ventricle. *J Physiol* **548**, 815–822.

Sah R, Ramirez RJ, Oudit GY, Gidrewicz D, Trivieri MG, Zobel C & Backx PH (2003). Regulation of cardiac excitation–contraction coupling by action potential repolarization: role of the transient outward potassium current (I_{to}). *J Physiol* **546**, 5–18.

Solaro RJ & Rarick HM (1998). Troponin and tropomyosin: proteins that switch on and tune in the activity of cardiac myofilaments. *Circ Res* **83**, 471–480.

Stull LB, Leppo MK, Marban E & Janssen PM (2002). Physiological determinants of contractile force generation and calcium handling in mouse myocardium. *J Mol Cell Cardiol* **34**, 1367–1376.

Stuyvers BD, McCulloch AD, Guo J, Duff HJ & Ter Keurs HE (2002). Effect of stimulation rate, sarcomere length and Ca^{2+} on force generation by mouse cardiac muscle. *J Physiol* **544**, 817–830.

Volk T & Ehmke H (2002). Conservation of L-type Ca^{2+} current characteristics in endo- and epicardial myocytes from rat left ventricle with pressure-induced hypertrophy. *Pflugers Arch* **443**, 399–404.

Volk T, Nguyen TH, Schultz JH & Ehmke H (1999). Relationship between transient outward K^+ current and Ca^{2+} influx in rat cardiac myocytes of endo- and epicardial origin. *J Physiol* **519**, 841–850.

Watanabe T, Delbridge LM, Bustamante JO & McDonald TF (1983). Heterogeneity of the action potential in isolated rat ventricular myocytes and tissue. *Circ Res* **52**, 280–290.

Wier WG (1990). Cytoplasmic $[Ca^{2+}]$ in mammalian ventricle: dynamic control by cellular processes. *Annu Rev Physiol* **52**, 467–485.

Williams DA & Fay FS (1990). Intracellular calibration of the fluorescent calcium indicator Fura-2. *Cell Calcium* **11**, 75–83.

Wokosin DL, Loughrey CM & Smith GL (2004). Characterization of a range of fura dyes with two-photon excitation. *Biophys J* **86**, 1726–1738.

Wood EH, Heppner RL & Weidmann S (1969). Inotropic effects of electric currents. I. Positive and negative effects of constant electric currents or current pulses applied during cardiac action potentials. II. Hypotheses: calcium movements, excitation-contraction coupling and inotropic effects. *Circ Res* **24**, 409–445.

Xu H, Guo W & Nerbonne JM (1999). Four kinetically distinct depolarization-activated K^+ currents in adult mouse ventricular myocytes. *J Gen Physiol* **113**, 661–678.

Zhou YQ, Foster FS, Parkes R & Adamson SL (2003). Developmental changes in left and right ventricular diastolic filling patterns in mice. *Am J Physiol Heart Circ Physiol* **285**, H1563–H1575.

Acknowledgements

This research was supported in part by start-up funds to W.R.G., provided by the Department of Medicine and the Institute of Molecular Medicine at the University of California, San Diego and by a Deutsche Forschungsgemeinschaft grant TE 391/1–1 to C.T. The authors are grateful to Dr Joan Heller Brown (Department of Pharmacology, UCSD) who graciously provided access to the Ionoptix myocyte shortening/Ca^{2+} system, to Dr Robert H Tukey (Department of Pharmacology, UCSD) for use of his Mx4000 Multiplex Quantitative PCR System (Stratagene) and to Dr Kenneth W Spitzer (Nora Eccles Harrisson Centre for cardiovascular Research and Training) for use of his myocyte edge tracking system (Crescent Electronic video edge detector, Phillips CCD camera).

Authors' present addresses

J. Chrast: Center for Integrative Genomics, University of Lausanne, Switzerland.

K. R. Chien: Cardiovascular Research Center, Massachusetts General Hospital, Boston, MA, USA.